Theor Chem Acc (2012) 131:1166
DOI 10.1007/s00214-012-1166-2

REGULAR ARTICLE

$[Zn_{10}(\mu_4\text{-}S)(\mu_3\text{-}S)_6(Py)_9(SO_4)_3]$ as a molecular model of ZnS surfaces: an experimental and theoretical study

Francesco Avanzini · Maurizio Casarin · Daniel Forrer · Luciano Pandolfo · Mauro Sambi · Andrea Vittadini

Received: 5 July 2011 / Accepted: 11 October 2011 / Published online: 2 March 2012

Abstract Experimental and theoretical results pertaining to $[Zn_{10}(\mu_4\text{-}S)(\mu_3\text{-}S)_6(Py)_9(SO_4)_3]$, a possible molecular model of ZnS S-terminated polar surfaces, as well as a potential source of strictly monodispersed ZnS quantum dots, are presented and discussed. The results of density functional theory (DFT) calculations provided a rationale for the peculiar arrangement of $[Zn_{10}(\mu_4\text{-}S)(\mu_3\text{-}S)_6(Py)_9(SO_4)_3]$ clusters in the solid state, contemporarily indicating the unsuitability of the isolated species to mimic whatever (polar or non-polar) ZnS surface. Despite the fact that such a failure is further confirmed by time-dependent DFT and UV–Vis diffuse reflectance spectroscopy, the combined use of theoretical outcomes, DRIFT measurements, and literature data pertaining to the surface chemical properties of ZnS (Hertl in Langmuir 4:594, 1988) ultimately testifies that $[Zn_{10}(\mu_4\text{-}S)(\mu_3\text{-}S)_6(Py)_9(SO_4)_3]$ is perfectly suited to model the interaction of pyridine molecules with ZnS surface Lewis acid sites. The herein reported theoretical results are expected to be a useful reference for the interpretation of chemisorption experiments of Py-based Lewis bases on single crystal ZnS surfaces.

Keywords Zinc sulfide · Chemisorption · Quantum dots · Density functional calculations

1 Introduction

When semiconductor nanocrystals have dimensions comparable to the Bohr exciton diameter, the spatial confinement of charge carriers gives rise to significant changes in the electronic properties of the material [1–4]. Further reductions in particle dimensions ultimately yield clusters of molecular size, which may provide, besides possible insights into the properties of the solid, an experimental validation of the cluster approach to the investigation of local phenomena in solids. Some of us have extensively used the molecular–cluster approach coupled to the density functional theory (DFT) to study solid-state phenomena [5–7], and, in this habit, we were able to single out molecular models of ZnO [8, 9],[1] ZnS [10], $Zn_4S(BO_2)_6$, and $Cd_4S(AlO_2)_6$ [11, 12], as well as of ZnS non-polar surfaces [13].

More than 10 years ago, Ali et al. [14] reported the synthesis and the structural characterization of a new type of zinc sulfide cluster ($[Zn_{10}(\mu_4\text{-}S)(\mu_3\text{-}S)_6(Py)_9(SO_4)_3]\cdot 3H_2O$, Py = pyridine) characterized by several fascinating peculiarities: (1) the occurrence of a neutral inorganic core ($[Zn_{10}(\mu_4\text{-}S)(\mu_3\text{-}S)_6(SO_4)_3]$, hereafter **IC**) constituted by a

Dedicated to Professor Vincenzo Barone and published as part of the special collection of articles celebrating his 60th birthday.

Electronic supplementary material The online version of this article (doi:10.1007/s00214-012-1166-2) contains supplementary material, which is available to authorized users.

F. Avanzini · M. Casarin (✉) · D. Forrer · L. Pandolfo · M. Sambi
Dipartimento di Scienze Chimiche DiSC, Università degli Studi di Padova, Padua, Italy
e-mail: maurizio.casarin@unipd.it

M. Casarin · D. Forrer · A. Vittadini
Istituto di Scienze e Tecnologie Molecolari, ISTM-CNR, V. Marzolo, 1, 35131 Padua, Italy

[1] A molecular model of a solid is a molecule or an ion whose stereochemistry and electronic structure reasonably mimic the structural arrangement and the nature of the valence (conduction) band top (bottom) of the solid itself [8].

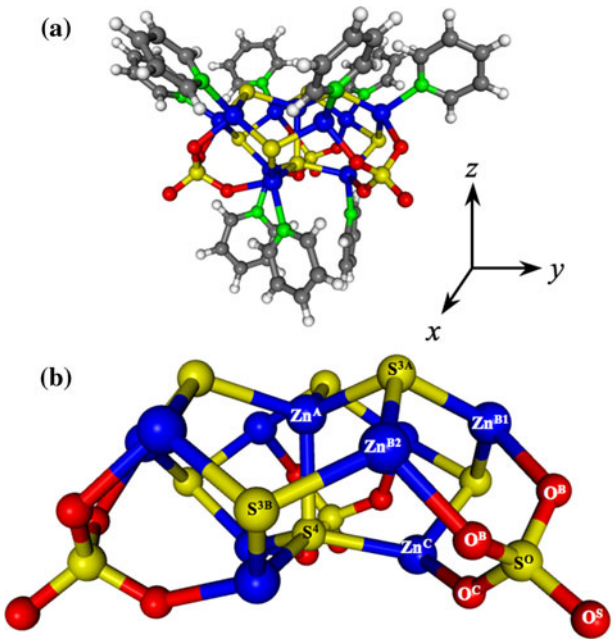

Fig. 1 Schematic representation of the $[Zn_{10}(\mu_4\text{-}S)(\mu_3\text{-}S)_6(Py)_9(SO_4)_3]$ cluster (**a**) and its kernel $Zn_{10}S_7$ capped by three tridentate SO_4^{2-} ligands (**b**). *Blue*, *yellow*, *red*, *green*, *gray*, and *white spheres* represent Zn, S, O, N, C, and H atoms, respectively; moreover, labels associated with the atoms of the $[Zn_{10}(\mu_4\text{-}S)(\mu_3\text{-}S)_6(SO_4)_3]$ inorganic core are the same proposed by Ali et al. [14] in their contribution

$Zn_{10}(\mu_4\text{-}S)(\mu_3\text{-}S)_6$ kernel capped by three SO_4^{2-} tridentate ligands (see Fig. 1) and distinguished by an unusual Zn–S connectivity neither corresponding to that of ZnS structural polymorphs (hexagonal wurtzite and cubic sphalerite) nor to the one of clusters formed by group 12 metals [15, 16]; (2) a singular supramolecular arrangement (see Fig. 2): the three Py molecules bonded to the Zn^C ions (Py^C) sink into the "basin" generated by the six Py ligands (Py^B) decorating the puckered ring of Zn^B ions of an adjacent cluster along the *a* axis[2]; (3) the presence of six $\mu_3\text{-}S^{2-}$ ions (S^{3A} and S^{3B} in Fig. 1b), each of them carrying a coordinative vacancy and trigonally coordinated to chemically complete Zn^{2+} ions which makes $[Zn_{10}(\mu_4\text{-}S)(\mu_3\text{-}S)_6(Py)_9(SO_4)_3]$ (hereafter **1**) a possible molecular model of ZnS, S-terminated, polar surfaces. Last but not least, **1** could represent a potential source of ZnS strictly monodispersed quantum dots having a diameter of $\sim$1 nm,[3] that is, significantly smaller than the ZnS excitonic Bohr radius (2.5 nm) [17].

[2] The Zn^B set can be further split in two three-member subsets (Zn^{B1} and Zn^{B2}) according to their higher or lower *z* coordinates with respect to the selected origin placed in S^4 in the adopted framework (see Fig. 1).

[3] Depyridination reactions at different temperature are in progress in our laboratory to identify $[Zn_{10}(\mu_4\text{-}S)(\mu_3\text{-}S)_6(Py)_9(SO_4)_3]\cdot 3H_2O$ decomposition products.

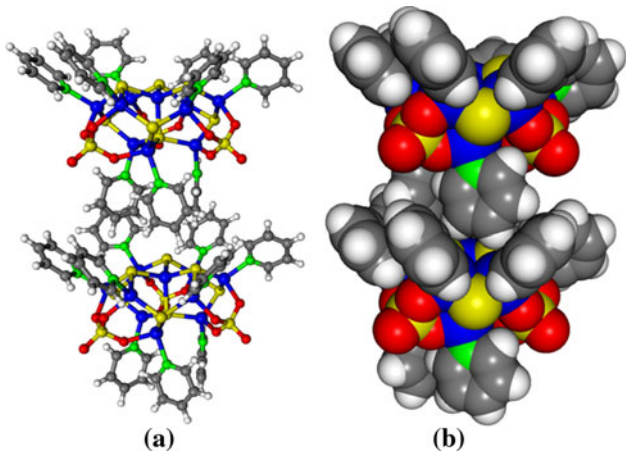

Fig. 2 Ball-and-stick (**a**) and space-filling (**b**) representations of two $[Zn_{10}(\mu_4\text{-}S)(\mu_3\text{-}S)_6(Py)_9(SO_4)_3]$ clusters along the *a*-axis. Water coordination molecules are not displayed for clarity

Despite all these features, neither experimental nor theoretical investigations of the electronic properties of **1** have been reported so far to our knowledge. In this contribution, the results of a series of DFT and time-dependent (TD) DFT numerical experiments on the isolated $[Zn_{10}(\mu_4\text{-}S)(\mu_3\text{-}S)_6(Py)_9(SO_4)_3]$ cluster are presented, discussed, and compared with the outcomes of diffuse reflectance spectroscopy measurements carried out in the UV–Vis and infrared wavelength ranges. The final goal of such a combined experimental and theoretical investigation is to obtain a rationale for the above described peculiarities.

2 Experimental and computational details

2.1 Chemicals, instrumentation, and syntheses

All solvents were distilled and degassed before use. PhSH, Et_3N, Me_4NCl, $ZnNO_3\cdot 6H_2O$, and S (Fluka) were used without further purification. GC/MS spectra of volatile products obtained in the thermal decomposition of $(Me_4N)_4[Zn_{10}(\mu_3\text{-}S)_4(\mu_2\text{-}SPh)_{12}(SPh)_4]$ (the precursor needed for the synthesis of $[Zn_{10}(\mu_4\text{-}S)(\mu_3\text{-}S)_6(Py)_9(SO_4)_3]\cdot 3H_2O$) were obtained on a FISONS MD 800 instrument equipped with a 30 ($\Phi = 0.25$ mm) capillary column, using He as carrier gas and EI ionization. Elemental analyses were provided by the Microanalysis Laboratory of the Department of Chemical Sciences of the University of Padova.

2.1.1 Synthesis of the $[Zn_{10}(\mu_3\text{-}S)_4(\mu_2\text{-}SPh)_{12}]$ precursor

The starting material to synthesize $[Zn_{10}(\mu_4\text{-}S)(\mu_3\text{-}S)_6(Py)_9(SO_4)_3]\cdot 3H_2O$ is the neutral cluster $[Zn_{10}(\mu_3\text{-}S)_4(\mu_2\text{-}SPh)_{12}]$, which has been prepared according to the

synthetic route reported in [13, 18]: $[NMe_4][Zn_{10}(\mu_3\text{-}S)_4(\mu_2\text{-}SPh)_{12}(SPh)_4]$ (906 mg, 0.32 mmol) was heated at 250 °C under dynamic vacuum (0.2 mmHg) for 5 h. GC/MS of the volatile collected revealed the presence of Me_3N and PhSMe. The residual solid (661 mg) corresponded to $[Zn_{10}(\mu_3\text{-}S)_4(\mu_2\text{-}SPh)_{12}]$ with a yield of 99%.

2.1.2 Synthesis of $Zn_{10}(\mu_4\text{-}S)(\mu_3\text{-}S)_6(Py)_9(SO_4)_3]\cdot 3H_2O$

The synthesis of $[Zn_{10}(\mu_4\text{-}S)(\mu_3\text{-}S)_6(Py)_9(SO_4)_3]\cdot 3H_2O$ was carried out according to a procedure slightly modified with respect to the one reported by Ali et al. [14]: $[Zn_{10}(\mu_3\text{-}S)_4(\mu_2\text{-}SPh)_{12}]$ (156 mg, 0.075 mmol) was dissolved in 15 mL of a solution prepared by treating 100 mL of pyridine with 500 mg of anhydrous Na_2SO_4; 36 mg of sulphur were then added. The mixture was heated at 70 °C under stirring, and sulphur dissolved in ca. 2 min yielding a yellow solution, which was cooled at room temperature (RT) and layered with 3 mL of acetone. The solution was left undisturbed for 4 weeks, yielding a cream-white solid, which was decanted, washed with pyridine, and dried under vacuum at RT. The obtained light yellow powder (17 mg, 9×10^{-3} mmol) implied a 12% yield. Elemental analysis: calculated for $[Zn_{10}(\mu_4\text{-}S)(\mu_3\text{-}S)_6(Py)_9(SO_4)_3]\cdot 3H_2O$: C = 27.97, H = 2.66, N = 6.52, S = 16.59; found: C = 27.07, H = 2.44, N = 6.27, S = 16.43.

2.2 Diffuse reflectance UV–Vis spectra

UV–Vis measurements were carried out on a Cary 5E spectrophotometer (Varian Inc., Palo Alto, CA), equipped with an integrating sphere coated with polytetrafluoroethylene. The employed setup allowed the exclusion of the specular component of the reflected light. Spectra were collected within the 300–800 nm wavelength range with a spectral resolution of 1 nm by using a self-supporting pellet.

2.3 Diffuse reflectance infrared Fourier transform (DRIFT) spectra

Fourier transform IR spectra were recorded with a Bruker Tensor 27 spectrophotometer by loading few milligrams of $[Zn_{10}(\mu_4\text{-}S)(\mu_3\text{-}S)_6(Py)_9(SO_4)_3]\cdot 3H_2O$ in the accessory for diffuse reflectance (Harrick Scientific) using KBr as a reference, and accumulating 32 scans at a resolution of 4 cm^{-1}. The collected spectra are displayed in Kubelka–Munk units [19, 20].

2.4 Numerical experiments

All the numerical experiments have been carried out by using the Amsterdam density functional package [21]. The geometry of **1** has been fully optimized without any symmetry constraint (C_1 symmetry point group), by adopting the hybrid GGA corresponding to the Becke's three parameters hybrid exchange [22] and to the Lee–Yang–Parr's correlation functional [23], and by adding a dispersion correction [24] (hereafter, DFT-D) to take care of possible van der Waals interactions between Py rings. A further series of numerical experiments without dispersion corrections (hereafter, DFT) have also been carried out for comparison. A 20% Hartree–Fock exchange has been adopted [25]. A triple-ζ Slater-type basis set plus a polarization function (TZP) have been used for all the atoms; furthermore, the inner core of Zn and S (1s–2p), O (1s), N (1s), and C (1s) atoms have been kept frozen throughout the calculations in a fully occupied configuration, excluding them from the variational space. Finally, the electronic structures have been studied with the aid of density of states (hereafter DOS) and partial DOS (PDOS) curves. To this end, we have used the Mulliken's prescription for partitioning the overlap density [26], and we have applied a 0.25 eV Lorentzian broadening factor to the one-electron eigenvalues.

Harmonic frequencies have been analytically calculated by using the dispersion corrected BP86 exchange–correlation functional. In fact, on one hand, the B3LYP functional has not yet been included among the functional allowing the analytical evaluation of harmonic frequencies [21][4]; on the other hand, the BP86 functional is known to provide a satisfactory agreement between experimental and theoretical frequencies [27–34]. Finally, low-lying electronic transitions of $[Zn_{10}(\mu_4\text{-}S)(\mu_3\text{-}S)_6(Py)_9(SO_4)_3]\cdot 3H_2O$ have been evaluated by coupling the TD-DFT [35] to the B3LYP exchange–correlation potential. TD-DFT calculations have been run by adopting the atomic coordinates derived from the solid-state structure.[5]

3 Results and discussion

The geometry of the title cluster significantly changes on passing from the $[Zn_{10}(\mu_4\text{-}S)(\mu_3\text{-}S)_6(Py)_9(SO_4)_3]\cdot 3H_2O$ crystal structure [14] to the isolated species (DFT-D and

[4] The computational cost of a numerical evaluation of vibrational frequencies by using the B3LYP exchange–correlation potential (787 single point runs) resulted prohibitive.

[5] TD-DFT calculations have been run by using geometrical parameters corresponding to the $[Zn_{10}(\mu_4\text{-}S)(\mu_3\text{-}S)_6(Py)_9(SO_4)_3]\cdot 3H_2O$ solid-state structure rather than employing the optimized geometry of **1**, because corresponding outcomes have been compared with the results of diffuse reflectance measurements carried out on a powder sample. In this regard, it is worthwhile to mention that, on passing from $[Zn_{10}(\mu_4\text{-}S)(\mu_3\text{-}S)_6(Py)_9(SO_4)_3]\cdot 3H_2O$ to **1**, besides a widening of the HOMO–LUMO energy difference (3.18 eV in the former case, 3.69 eV in the latter), DOS and PDOS are very similar.

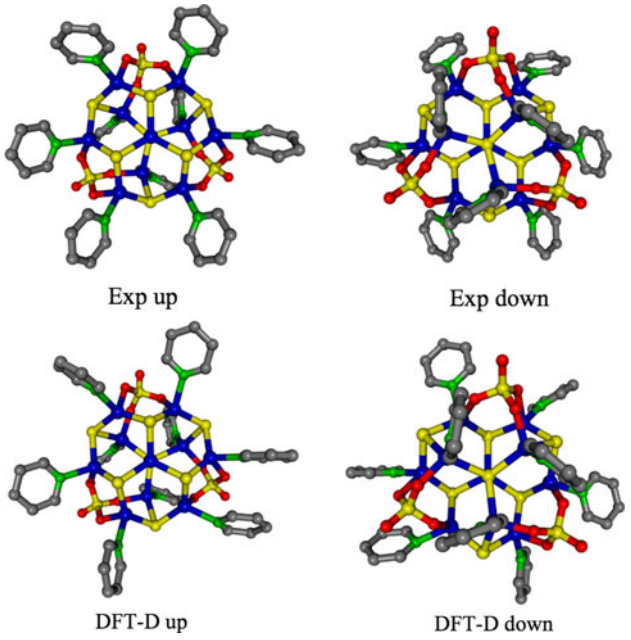

Fig. 3 Comparison of the $[Zn_{10}(\mu_4\text{-}S)(\mu_3\text{-}S)_6(Py)_9(SO_4)_3]$ experimental (Exp) and optimized (DFT-D) molecular arrangements along the *a*-axis

DFT optimized Cartesian coordinates of **1** are reported in the Online Resource 1 and 2, respectively), though the pseudo threefold axis is conserved. Variations mainly involve the relative orientation of Py^B molecules, which could be expected, given the supramolecular arrangement of $[Zn_{10}(\mu_4\text{-}S)(\mu_3\text{-}S)_6(Py)_9(SO_4)_3]\cdot 3H_2O$. On the other hand, both **IC** and the relative orientation of the three Py^C ligands undergo only minor perturbations upon optimization. Geometry modifications of **1** are better appreciated by referring to Fig. 3, which shows that at least three competing interactions contribute to determine the arrangement of Py^B ligands : (1) the H-bonding between C_α^{Py} H atoms and the unsaturated $\mu_3\text{-}S^{3A}$ ions (mainly involving Zn^{B1}-coordinated Py^B); (2) the H-bonding between C_α^{Py} H atoms and the SO_4^{2-} fragments (mainly involving Zn^{B2}-coordinated Py^B)[6]; (3) the π–π interaction between adjacent pyridine molecules. Obviously, the last interaction is absent in DFT calculations (the reader may refer to the Online Resource 2). Despite the fact that $\mu_3\text{-}S^{3B}$ ions represent a source of negative electrostatic potential comparable to $\mu_3\text{-}S^{3A}$ (see Fig. 4),[7] their role in determining the orientation of pyridine molecules seems to be negligible. In addition to that, the color-mapped molecular electrostatic potential (MEP) superimposed on the 3D map of the density matrix of **1** ultimately testifies that electrostatic interactions play an important role in determining the head–tail aggregation of **1** along *a* in $[Zn_{10}(\mu_4\text{-}S)(\mu_3\text{-}S)_6(Py)_9(SO_4)_3]\cdot 3H_2O$. As far as **IC** is concerned, bond distances and bond angles reported in Table 1 confirm that the inorganic core of **1** undergoes only minor perturbations on passing from the $[Zn_{10}(\mu_4\text{-}S)(\mu_3\text{-}S)_6(Py)_9(SO_4)_3]\cdot 3H_2O$ crystal structure [14] to the isolated cluster.

Before moving to the analysis of the electronic structure of **1**, a few words about the negligible effects of the geometry optimization on the relative arrangement of Py^C molecules are needed. As a matter of fact, a thorough inspection of the Py^C environment stresses that, both in the crystal structure and in the isolated cluster, each of them is constrained between two contiguous SO_4^{2-} ligands. More specifically, for a particular Zn^C ion (say Zn^{C1}), its four coordinative positions are occupied by S^4, S^{3C1}, O^{C1}, and the pyridine molecule Py^{C1} whose C_α^{Py} H atoms are H-bonded to the O atoms of two contiguous SO_4^{2-} ions: the former H-bonding involves O^{C1}, while the latter implies an O^B of the adjacent SO_4^{2-} group.[8]

DOS and PDOS of **1** are displayed in Figs. 5 and 6, where DOS main features have been alphabetically labeled. The inspection of both figures indicates that (1) the feature **C** is originated by **IC**-based occupied MOs, mainly localized on S and O atomic orbitals (AOs) and with negligible contributions from Py molecules; (2) the HOMOs, generating the evident shoulder on the higher energy side of **C**, account for linear combinations of S^{3A} lone pairs (n^{S3A}, see Fig. 6a); (3) the LUMOs, generating the feature **D**, correspond to $^{Py}\pi^*$ MOs. According to this picture, the low-energy region of the UV–Vis spectrum of **1** should be dominated by $n^S \rightarrow {}^{Py}\pi^*$ and $n^O \rightarrow {}^{Py}\pi^*$ electronic excitations.

In Fig. 7 the UV–Vis diffuse reflectance spectrum of $[Zn_{10}(\mu_4\text{-}S)(\mu_3\text{-}S)_6(Py)_9(SO_4)_3]\cdot 3H_2O$ is displayed. The experimental pattern in the wavelength range extending from 300 to 600 nm (the instrumental setup prevents any measurement at wavelengths shorter than 300 nm) is characterized by the presence of an evident shoulder **S**, extending from 550 to 420 nm, and the band **A** centered at ~310 nm. TD-DFT calculations indicate that the lowest 30 excitations[9] cover an energy range of ~0.6 eV, from 2.66 (466 nm) to 3.23 eV (384 nm), and mainly imply

[6] Geometrical parameters reported in the Online Resource 1 certainly correspond to a local minimum, and it seems reasonable to assume that the potential energy surface includes many of them.

[7] The mean values of the S^{3A} and S^{3B} Mulliken [26] (Hirshfeld) [36] gross atomic charges amount to -0.48 (-0.33) and -0.46 (-0.31), respectively.

[8] Experimental (optimized) $H(C_\alpha^{Py})\cdots O^C$ and $H(C_\alpha^{Py})\cdots O^B$ internuclear distances are 2.668, 2.563, 2.551 Å (2.473, 2.450, 2.379 Å) and 2.752, 2.663, 2.619 Å (2.204, 2.174, 2.147 Å), respectively.

[9] The absence of any symmetry constraint and the use of a TZP basis set for all the atoms imply a very large number (475,881) of possible excitations to be computed. The available computational resources allowed us to evaluate the first 30.

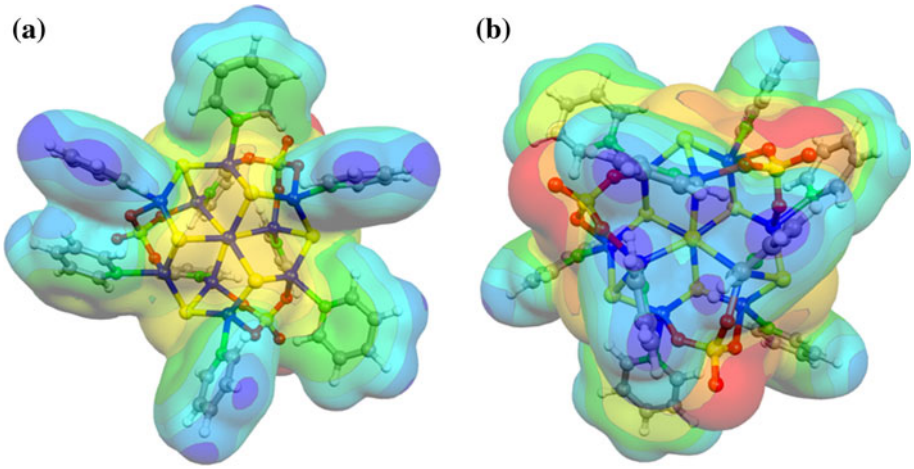

Fig. 4 Up (**a**) and down (**b**) 3D MEP map superimposed on the density matrix of **1**. The *red* (*blue*) MEP region corresponds to a negative (positive) potential of −0.09 (0.05) au. The reported isodensity surface is 0.001 $Å^{-3}$

Table 1 Selected mean internuclear distances (Å) and bond angles (°) of the $Zn_{10}S_7(SO_4)_3$ inorganic core of the $[Zn_{10}S_7(py)_9(SO_4)_3]$ cluster

	Theory	Experiment[a]
Zn^A–S^4	2.464	2.453
Zn^C–S^4	2.390	2.321
Zn^A–S^{3A}	2.381	2.339
Zn^B–S^{3A}	2.306	2.278
Zn^B–S^{3B}	2.317	2.285
Zn^B–N^B	2.165	2.060
Zn^C–N^C	2.111	2.059
Zn^C–O^C	2.038	2.006
Zn^B–O^B	2.070	2.033
S^4–Zn^A–S^{3A}	110.0	107.7
S^{3A}–Zn^A–S^{3A}	108.9	111.2
S^{3A}–Zn^B–S^{3B}	132.1	124.6
S^4–Zn^C–S^{3B}	119.8	120.2
Zn^A–S^4–Zn^C	105.8	103.3
Zn^C–S^{3B}–Zn^B	87.5	92.0
Zn^C–S^4–Zn^C	112.9	114.9
Zn^B–S^{3A}–Zn^B	93.1	101.9
Zn^A–S^{3A}–Zn^B	96.3	103.2
Zn^B–S^{3B}–Zn^B	101.1	106.8
S^4–Zn^C–O^C	113.0	106.4
S^4–Zn^C–N^C	106.2	108.9
S^{3B}–Zn^C–O^C	104.7	109.3
S^{3B}–Zn^C–N^C	118.9	113.8
O^C–Zn^C–N^C	90.3	95.2
O^B–Zn^B–N^B	91.2	95.6
S^{3B}–Zn^B–O^B	98.4	102.3
S^{3A}–Zn^B–O^B	116.2	111.7
S^{3B}–Zn^B–N^B	108.5	112.5
S^{3A}–Zn^B–N^B	103.1	106.0

[a] After Ref. [13]

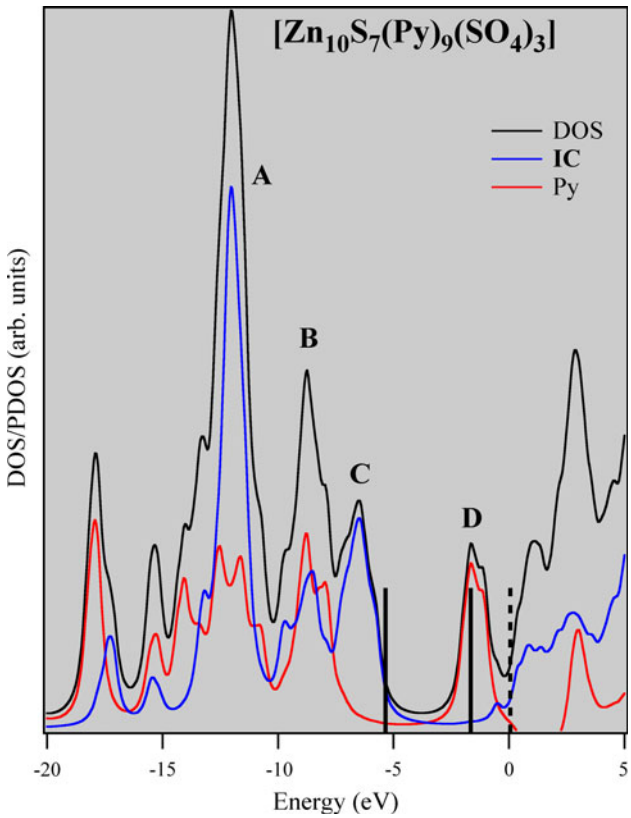

Fig. 5 DOS and PDOS of **1**. Vertical solid lines account for the HOMO and LUMO energies; the *dashed vertical line* corresponds to the energy of the lowest-unoccupied MO having a localization on Zn 4s empty AOs larger than 1.0%

$n^S \rightarrow {}^{Py}\pi^*$ transitions. This result, coupled with the Mulliken population analysis pertaining to the outermost occupied levels of **1** (see Figs. 5 and 6; see footnote 5), justifies the tentative assignment of spectral features **S** and **A** to $n^S \rightarrow {}^{Py}\pi^*$ and $n^O \rightarrow {}^{Py}\pi^*$ $[Zn_{10}(\mu_4\text{-}S)(\mu_3\text{-}S)_6(Py)_9(SO_4)_3]\cdot 3H_2O$ transitions, respectively.

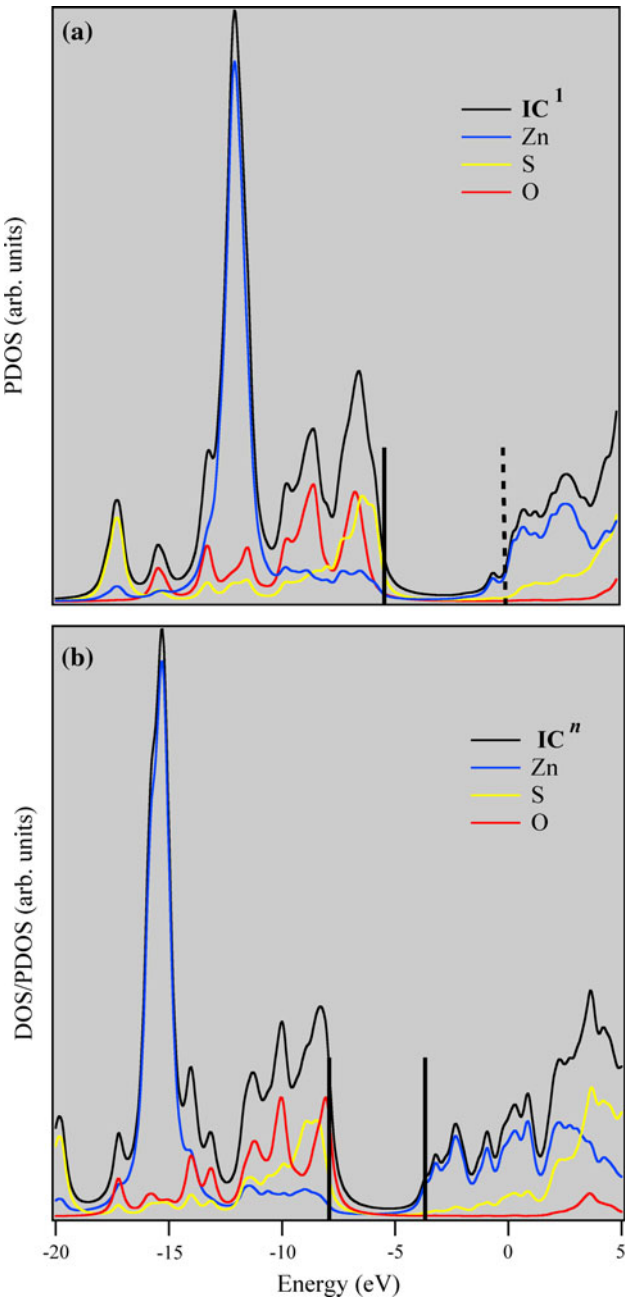

Fig. 6 **IC** PDOS (**a**) and **IC**^{n} DOS (**b**). The physical meaning of the *vertical solid* and *dashed lines* is the same of Fig. 5

The strict application of the molecular model definition (see footnote 1) implies that **1** cannot be considered well tailored to mimic either polar or non-polar ZnS surfaces; however, if anything, a reasonable model of a ZnS surface characterized by the presence of Lewis acid sites (L_S^a, the surface cations Zn^B and Zn^C) and Lewis base sites (the surface anions S^{3A} and S^{3B}) with Py molecules coordinately bound to L_S^a. In this regard, it is noteworthy that, in the late 1988 [37], W. Hertl investigated by DRIFT spectroscopy the interaction of ZnS surfaces with different

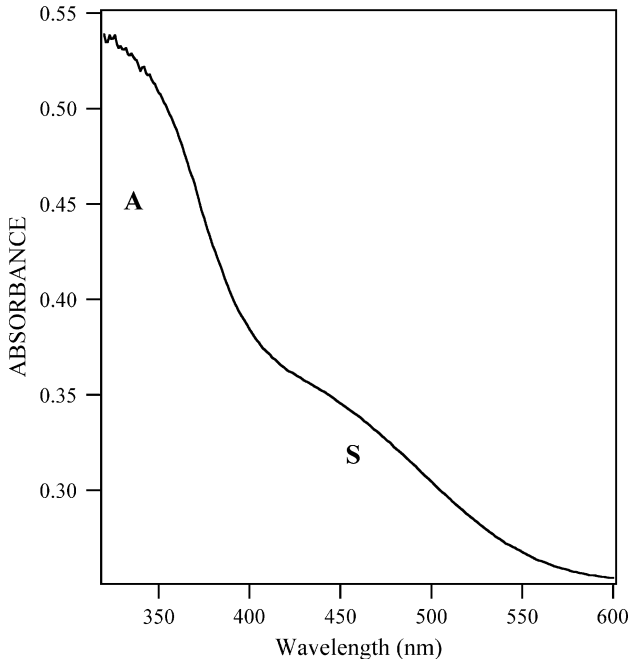

Fig. 7 Diffuse reflectance UV–Vis spectrum of $[Zn_{10}(\mu_4\text{-}S)(\mu_3\text{-}S)_6(Py)_9(SO_4)_3]\cdot 3H_2O$ in the wavelength range 300–600 nm

Lewis bases (Py and NH_3) with the aim of discriminating their interaction with proton-donating surface Brønsted acids and surface L_S^a. Peaks due to the pyridine coordinately bound to L_S^a were revealed at 1,448, 1,490, 1,570, and 1,609 cm^{-1} [37]. Interestingly, the DRIFT spectrum of $[Zn_{10}(\mu_4\text{-}S)(\mu_3\text{-}S)_6(Py)_9(SO_4)_3]\cdot 3H_2O$ in the same energy range reported by W. Hertl (1,800–1,300 cm^{-1}, see Fig. 8a) is characterized by four well evident and rather narrow peaks centered at 1,452, 1,489, 1,572, and 1,607 cm^{-1}[10] satisfactorily reproduced by dispersion corrected BP86 calculations[11] (see Fig. 8b). In this regard, the analysis of normal mode eigenvectors clearly indicates that each peak numerically labeled in Fig. 8b is generated by nine closely spaced normal modes corresponding to symmetric ($\nu_{1,588}$ and $\nu_{1,462}$) and antisymmetric ($\nu_{1,557}$ and $\nu_{1,452}$) stretchings of Py rings. Moreover, $\nu_{1,588}$ and $\nu_{1,462}$ ($\nu_{1,557}$ and $\nu_{1,452}$) symmetric (antisymmetric) vibrations involve the L_S^a–N stretchings (S–L_S^a–N and O–L_S^a–N bendings). As a whole, besides a confirmation of the assignment proposed by Hertl for DRIFT bands associated with Py molecules coordinately bound to ZnS L_S^a, the results herein presented ultimately proves that $[Zn_{10}(\mu_4\text{-}S)(\mu_3\text{-}S)_6(Py)_9(SO_4)_3]\cdot 3H_2O$ is a very well-tailored molecular model of Py molecules interacting with surface ZnS L_S^a.

[10] The broad band centered at 1,655 cm^{-1} and exhibiting some structure is revealed in the H–O–H bending region.

[11] The optimized geometry of **1** at dispersion-corrected B3LYP and BP86 levels are almost indistinguishable.

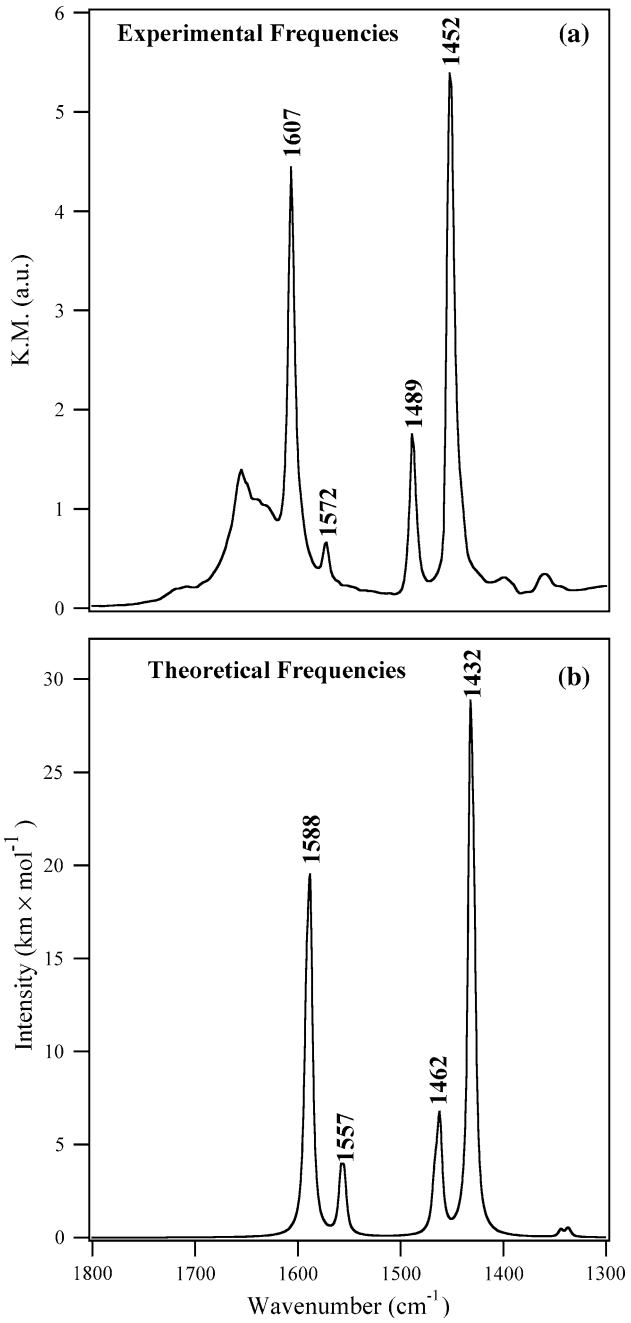

Fig. 8 **a** DRIFT spectrum of $[Zn_{10}(\mu_4\text{-}S)(\mu_3\text{-}S)_6(Py)_9(SO_4)_3]\cdot 3H_2O$ in the 1,300–1,800 cm^{-1} energy range; **b** theoretical frequencies, analytically evaluated, of $[Zn_{10}(\mu_4\text{-}S)(\mu_3\text{-}S)_6(Py)_9(SO_4)_3]$ in the 1,300–1,800 cm^{-1} energy range

It has been already mentioned that **1** could represent a potential source of ZnS strictly monodispersed quantum dots. In order to look into such a hypothesis from a theoretical point of view, the **IC** PDOS of **1** (**IC**$^{\mathbf{1}}$) has been compared with the DOS of the naked-**IC** (**IC**$^{\boldsymbol{n}}$) cluster.[12]

[12] A further series of B3LYP-D numerical experiments on **IC**$^{\boldsymbol{n}}$ (**1** with no Py ligand) have been carried out by using the optimized coordinates of **1**.

The inspection of Fig. 6 clearly testifies that the removal of Py molecules determines a general, but not uniform, shift toward more negative energies of the **IC**-based energy levels. In more detail, the largest shift ($\sim$3.5 eV) involves the Zn-based energy levels, while the smallest one ($\sim$1.5 eV) implicates the O-based states. Such a reorganization of the **IC** electronic structure implies: (1) a different localization of HOMOs on passing from **IC**$^{\mathbf{1}}$ to **IC**$^{\boldsymbol{n}}$, mainly concentrated on n^{S3A} in the former case, strongly localized on n^{O} in the latter; (2) the narrowing of the ΔE between the **IC** HOMOs and the lowest states with a significant localization on Zn 4s AOs (the **IC**$^{\boldsymbol{n}}$ LUMOs). Incidentally, the **IC**$^{\boldsymbol{n}}$ HOMO–LUMO ΔE amounts to 4.2 eV. Now, the use of the relation proposed by Suyver et al. [38] to correlate nanoparticle radii (nm) and band gap ΔE (eV) for nanocrystalline ZnS,

$$r(\Delta E) = \frac{0.32 - 2.9 \times \sqrt{\Delta E - 3.49}}{2 \times (3.50 - \Delta E)}$$

would imply, with $\Delta E = 4.2$ eV, a $r(\Delta E) \sim 1.5$ nm, in qualitative agreement with the **IC** dimensions ($r = 0.7$–0.8 nm). Such a result corroborates the hypothesis that **1** could represent a potential starting material to get ZnS strictly monodispersed quantum dots with a diameter of the order of magnitude of 1 nm, contemporarily spurring the need of looking into its chemical reactivity (see footnote 3).

4 Conclusions

In this contribution, we have presented the results of an experimental and theoretical study of the electronic structure of $[Zn_{10}(\mu_4\text{-}S)(\mu_3\text{-}S)_6(Py)_9(SO_4)_3]$, a neutral zinc sulfide cluster characterized by the presence of two kinds of sulfide ions: a μ_4-S^{2-} tetrahedrally coordinated to four chemically complete Zn^{2+} cations and six μ_3-S^{2-} each of them trigonally coordinated to three chemically complete Zn^{2+} cations and contemporarily carrying a coordinative vacancy. Despite such a structural arrangement, the combined use of DFT-D, TD-DFT, and UV–Vis diffuse reflectance spectroscopy underlines the inability of $[Zn_{10}(\mu_4\text{-}S)(\mu_3\text{-}S)_6(Py)_9(SO_4)_3]$ to mimic the electronic properties of an extended ZnS surface, polar or non-polar. Nevertheless, theoretical outcomes and the results of DRIFT measurements ultimately testify that $[Zn_{10}(\mu_4\text{-}S)(\mu_3\text{-}S)_6(Py)_9(SO_4)_3]$ is perfectly suited to model the interaction of Py molecules with ZnS surface L_S^a, thus confirming the assignment proposed by Hertl for DRIFT bands associated to Py molecules coordinately bound to ZnS L_S^a. Theoretical outcomes herein reported might then be useful in the future to drive the rationalization of experimental evidences concerning the chemisorption of Lewis bases,

such as pyridine, on single crystal ZnS surfaces. As a whole, the comparison with literature data [10, 11, 13] confirms and reinforces our belief that identical or very similar cluster skeletons do not necessarily imply equivalent or very similar cluster electronic properties; the suitability of specific systems to be molecular models of extended solids has to be verified for each single case.

Acknowledgments Computational resources and assistance were provided by the "Laboratorio Interdipartimentale di Chimica Computazionale" (LICC) at the Department of Chemistry of the University of Padova. Molecular graphics has been generated by Molekel [39].

References

1. Wang Y, Herron N (1991) J Phys Chem 95:525
2. Weller H (1993) Angew Chem Int Ed Engl 32:41
3. Henglein A (1997) Ber Bunsenges Phys Chem 101:1562
4. Hamad S, Woodley SM, Catlow CRA (2009) Mol Simulat 35:1015
5. Casarin M, Maccato C, Vittadini A (1997) Surf Sci 377:587
6. Casarin M, Maccato C, Vittadini A (1998) Inorg Chem 37:5842
7. Casarin M, Falcomer D, Glisenti A, Vittadini A (2003) Inorg Chem 42:436
8. Bertoncello R, Bettinelli M, Casarin M, Gulino A, Tondello E, Vittadini A (1992) Inorg Chem 31:1558
9. Casarin M, Tondello E, Calderazzo F, Vittadini A, Bettinelli M, Gulino A (1993) J Chem Soc, Faraday Trans 89:4363
10. Albinati A, Casarin M, Eisentraeger F, Maccato C, Pandolfo L, Vittadini A (2000) J Organomet Chem 593–594:307
11. Albinati A, Casarin M, Maccato C, Pandolfo L, Vittadini A (1999) Inorg Chem 38:1145
12. Casarin M, Maccato C, Vittadini A (2002) J Phys Chem B 106:2569
13. Bertoncello R, Bettinelli M, Casarin M, Maccato C, Pandolfo L, Vittadini A (1997) Inorg Chem 36:4707
14. Ali B, Dance IG, Craig DC, Scudder ML (1998) J Chem Soc Dalton Trans 1661
15. Dance IG, Fisher KJ (1994) Prog Inorg Chem 41:637
16. Archibald SJ (2003) In: McCleverty JA, Meyer TJ (eds) Comprehensive coordination chemistry II, vol 6. p 1148
17. Biggs MM, Ntwaeaborwa OM, Terblans JJ, Swart HC (2009) Phys B 404:4470
18. Farneth WE, Herron N, Wang Y (1992) Chem Mater 4:916
19. Kubelka P, Munk F (1931) Z Tech Phys 12:593
20. Kortum G (1969) Reflectance spectroscopy. Springer, New York
21. Amsterdam Density Functional (ADF) version 2010. http://www.scm.com
22. Becke AD (1993) J Chem Phys 98:5648
23. Lee C, Yang W, Parr RG (1988) Phys Rev B 37:785
24. Grimme S (2006) J Comput Chem 27:1787
25. Stephens PJ, Devlin FJ, Chabalowski CF, Frisch MJ (1994) J Phys Chem 98:11623
26. Mulliken RS (1955) J Chem Phys 23:1833
27. Casarin M, Maccato C, Vittadini A (1998) J Phys Chem B 102:10745
28. Casarin M, Pandolfo L, Vittadini A (2001) Organometallics 20:754
29. Casarin M, Pandolfo L, Sassi A (2002) Organometallics 21:2235
30. Casarin M, Maccato C, Vittadini A (2002) J Phys Chem B 106:795
31. Casarin M, Vittadini A (2003) Phys Chem Chem Phys 5:2461
32. Casarin M, Falcomer D, Glisenti A, Vittadini A (2003) Inorg Chem 42:436
33. Casarin M, Corvaja C, Di Nicola C, Falcomer D, Franco L, Monari M, Pandolfo L, Pettinari C, Piccinelli F, Tagliatesta P (2004) Inorg Chem 43:5865
34. Casarin M, Pandolfo L, Vittadini A (2009) Phys Chem Chem Phys 11:94
35. Gross EKU, Dobson JF, Petersilka M (1996) In: Nalewajski RF (ed) Density functional theory. Springer, Heidelberg
36. Hirshfeld FL (1977) Theor Chim Acta 44:129
37. Hertl W (1988) Langmuir 4:594
38. Suyver JF, Wuister SF, Kelly JJ, Meijerink A (2001) Nano Lett 1:429
39. Varetto U MOLEKEL 5.4.0.8, Swiss National Supercomputing Centre: Manno (Switzerland)